ChemPubSoc Europe

DOI: 10.1002/chem.201301724

CHEMISTRY
A European Journal
Full Paper

Nanostructures

Pt_3Co Concave Nanocubes: Synthesis, Formation Understanding, and Enhanced Catalytic Activity toward Hydrogenation of Styrene

Chenyu Wang,[a] Cuikun Lin,[b] Lihua Zhang,[c] Zewei Quan,[a] Kai Sun,[d] Bo Zhao,[b] Feng Wang,[e] Nathan Porter,[a] Yuxuan Wang,[f] and Jiye Fang*[a, f]

Abstract: We report a facile synthesis route to prepare high-quality Pt_3Co nanocubes with a concave structure, and further demonstrate that these concave Pt_3Co nanocubes are terminated with high-index crystal facets. The success of this preparation is highly dependent on an appropriate nucleation process with a successively anisotropic overgrowth and a preservation of the resultant high-index planes by control binding of oleyl-amine/oleic acid with a fine-tuned composition. Using a hydrogenation of styrene as a model reaction, these Pt_3Co concave nanocubes as a new class of nanocatalysts with more open structure and active atomic sites located on their high-index crystallographic planes exhibit an enhanced catalytic activity in comparison with low-indexed surface terminated Pt_3Co nanocubes in similar size.

Introduction

The hydrogenation of organic compounds is a class of very important reactions. An addition of hydrogen to double and/or triple bonds in hydrocarbons could, for example, be involved in gasoline manufacture, as well as conversion of coal into liquid fuels. It has been well understood that a hydrogenation involves a process of adsorption of molecules, scission of C–C bonds, and disassociation of products from special sites of high reactivity, denoted as active centres, on the surface of catalysts. For a catalyst study, hydrogenation of olefins has simply been a probe reaction for evaluation of heterogeneous catalysts, especially noble metals (such as Pt, Pd, and Au), which are widely used in petrochemical, pharmaceutical, and fine agricultural-chemical industries.[1] It was known that each crystallographic facet of a catalyst has its own peculiarities for catalytic activity. Investigations have been conducted to search for the most active sites or crystallographic planes with ensembles of such atomic sites. For example, {111} planes of Au preferentially activate C=O group, whereas its low-coordinated sites mostly locating at corners and edges favor the breaking of C=C bonds.[2] It was also determined that a hydrogenation of styrene takes place on defect sites (high-index kinks and steps) of Pd catalysts, rather than their low-index terraces.[3] Investigations indicate that catalysts bounded with high-index facets contain high density of low-coordinated atoms and exhibit ubiquitous catalytic ability on electro-oxidation of small organic molecules,[4–8] and should be the best promoter for the hydrogenation of olefins.

It is known that decrease of catalyst size to a nanometer scale could maximize the surface area and possibly the number of active sites for enhancing the catalytic performance.[9] However, most studies on nanocatalyst activity still rely on a decrease of their particle size, which could generate more corners and edges.[10] Further development of synthesis approaches in shape-controlled nanocatalysts, that is, nanopolyhedra, is therefore expected. In this regard, it is promising to fabricate and investigate nanocatalysts with high-index crystallographic facets that contain more low-coordinated atoms in steps, edges, and kinks.[11–12] Although it has been demonstrated that chemical properties, especially the catalytic performance of metallic nanocrystals (NCs), are significantly dependent on their size, composition, and morphology,[13–15] study on shape-controlled nanocatalysts with high-index crystallographic facets toward hydrogenation reactions is still in its infancy.

High-index nanopolyhedra could present in either concave or non-concave morphologies.[12] A few classes of non-concave

[a] C. Wang, Dr. Z. Quan,[+] N. Porter, Prof. Dr. J. Fang
Department of Chemistry, State University of New York at Binghamton
Binghamton, New York 13902 (USA)
Fax: (+1) 607-777-4478
E-mail: jfang@binghamton.edu

[b] Dr. C. Lin, Dr. B. Zhao
Department of Chemistry, University of South Dakota
Vermillion, South Dakota 57069 (USA)

[c] Dr. L. Zhang
Center for Functional Nanomaterials, Brookhaven National Laboratory
Upton, New York 11973 (USA)

[d] Dr. K. Sun
Department of Materials Science and Engineering
University of Michigan, Ann Arbor, Michigan 48109 (USA)

[e] Dr. F. Wang
Department of Sustainable Energy Technology
Brookhaven National Laboratory, Upton, New York 11973 (USA)

[f] Dr. Y. Wang, Prof. Dr. J. Fang
Materials Science and Engineering Program
State University of New York at Binghamton
Binghamton, New York 13902 (USA)

[+] Present address: EES-14 and MPA-MSID, Los Alamos National Laboratory
Los Alamos, New Mexico 87545 (USA)

Supporting information for this article is available on the WWW under http://dx.doi.org/10.1002/chem.201301724.

noble metal NCs with high-index crystallographic facets, such as Pt tetrahexahedron NCs[16] with {*h k* 0} facets and Pd trapezohedron NCs[17] have been prepared by using an electrochemical method. However, their size is larger than 100 nm. On the other hand, several research groups recently demonstrated their solution-based synthesis of small-sized concave noble metal NCs, such as Pt,[18–19] Pd,[4,20] Rh,[21] Au/Pd,[22] Pt/Fe,[23] and Pt/Pd[24] with various notable electrocatalytic performance. To the best of our knowledge, few hydrogenation studies by using high-index nanocatalysts have been reported. Furthermore, few classes of bimetallic NCs with high-index surfaces have been synthesized. Bearing in mind that incorporation of less expensive transition metals (such as Co, Fe, and Ni) into noble metal to form high-index facet-bounded bimetallic NCs will not only reduce the overall preciousness but also endow them with superior catalytic performance due to their modified surface electronic structure, bimetallic NCs with high-index crystallographic facets are anticipated to exhibit superior catalytic behavior (see below). Herein, we report a robust synthesis of Pt_3Co concave nanocubes with high-index crystallographic surfaces, as well as their enhanced catalytic activity toward hydrogenation of styrene.

Results and Discussion

Figure 1a depicts a transmission electron microscope (TEM) image of Pt_3Co NCs, showing that most NCs possess cubic morphology with curved surfaces as shown in a 3D perspective illustration presented in Figure 1b. The average size of these NCs, determined from their side length of TEM projective images, was measured as 11.8 ± 1.0 nm. Figure 1a also indicates that the region close to the center in each of the dominant NCs exhibits lighter contrast in comparison with the area near the edges, confirming the concave morphology. In Figure 1c, a high-resolution TEM (HRTEM) image projected along the $<100>$ zone axis on a typical Pt_3Co NC, as was confirmed by the corresponding Fourier transform pattern (Figure 1d), indicates an average *d* spacing of 0.193 nm on the basis of a measurement on more than 12 adjacent lattice fringes. For a concave nanocube enclosed by high-index facets, their Miller indices can be derived from the projection angles along a selected crystallographic axis.[4,19,24,25] As illustrated in Figure 1c, angles between four high-index-enclosed concave facets and the {100} facets of an ideal cube were determined as 25, 30, 28, 22, 34°…, further suggesting that the Miller indices of these actual surfaces are different from those of the basal planes, that is, low-index facets {100}, {110}, and {111}. Stepped surface consisting of {100} terraces and {110} steps can be readily revealed in the HRTEM image (Figure 1e). As shown in Figure 1e, each of the concave surface is a mixture of several {*h k* 0} facets instead of being composed of sub-facets with a fixed Miller index.

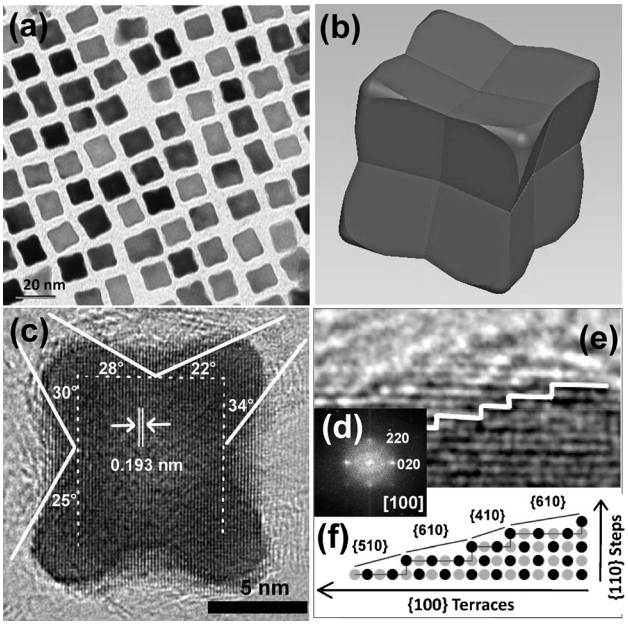

Figure 1. TEM images of Pt_3Co concave nanocubes: a) as-prepared Pt_3Co concave nanocubes; b) 3D perspective illustration model of a concave cube; c) HRTEM of a single Pt_3Co concave nanocube; d) Fourier transform pattern of the concave nanocube shown in (c); e) stepped surface highlighted from the HRTEM image; f) scheme of the stepped surface composed of a mixture of high-index facets with {100} terraces and {110} steps.

The above-mentioned average *d* spacing is close to that of Pt_3Co (200) according to ICDD PDF card 29–0499. Elemental mapping on a selected concave nanocube obtained by high-angle annular dark-field scanning TEM-energy dispersive X-ray (HAADF-STEM-EDS; Figure S1 in the Supporting Information) suggests that the Pt and Co were evenly distributed in the NC, confirming a bimetallic structure in this alloy. The Pt/Co chemical composition in the concave nanocubes was further evaluated by using an inductively coupled plasma-optical emission spectrometry (ICP-OES) technique. As indicated in Table S2 in the Supporting Information, the ICP analysis result suggests that the molar ratio between Pt and Co is close to 72:28.[26] For the purpose of simplicity, we refer the composition as Pt_3Co in the present work. To confirm the microstructure of these Pt_3Co concave nanocubes, XRD patterns were recorded and presented in Figure 2. By indexing all the detectable sharp peaks in the XRD pattern of as-prepared Pt_3Co concave nanocubes (Figure 2a) by using standard Pt_3Co pattern from ICDD PDF card 29–0499 (Figure 2, bottom), it confirms that these NCs possess a highly crystalline face-cantered cubic (fcc) phase. No diffraction signal of either single Pt or Co was detected, further indicating that only a single Pt_3Co phase exists in the sample. When these concave nanocubes were carefully deposited on a surface-polished Si wafer, the (200) diffraction peak was enhanced apparently (Figure 2b). This indicates that these Pt_3Co concave nanocubes have a highly symmetric morphology and could be aligned perfectly flat on the surface of the substrate with (100) texture, as was discussed previously.[27–29] The XRD pattern determined from the sample after a catalytic reaction does not show any detectable change and more discussion will be given shortly (Figure 2c).

To get a deep insight into the formation mechanism of the Pt_3Co nanocubes with a concave structure, we designed and implemented a group of experiments with a variation of several parameters including oleylamine (OAM)/oleic acid (OA)

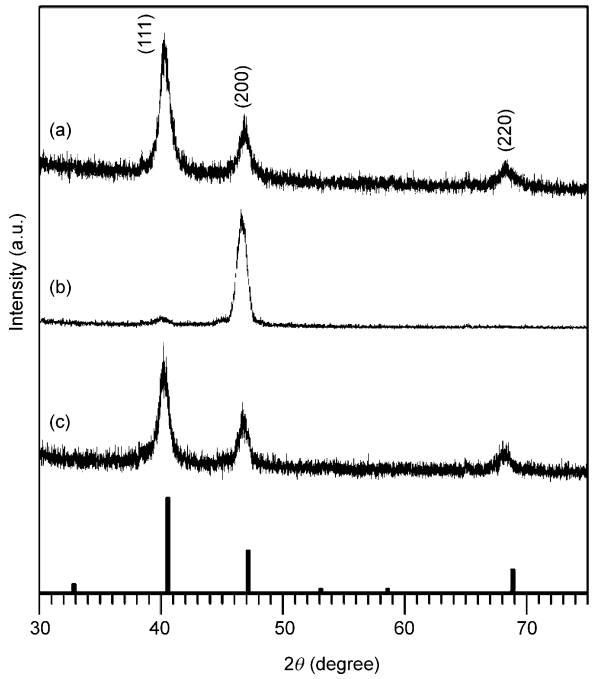

Figure 2. XRD patterns of Pt_3Co concave nanocubes. a) As-prepared Pt_3Co concave nanocubes randomly deposited on a PANalytical zero-background Si sample holder; b) same sample assembled on a surface-polished 25 mm Si $<100>$ wafer; c) Pt_3Co sample measured after a catalytic reaction of styrene hydrogenation on the PANalytical sample holder. The lines on the bottom represent a standard bulk Pt_3Co XRD pattern (ICDD PDF card 29-0499).

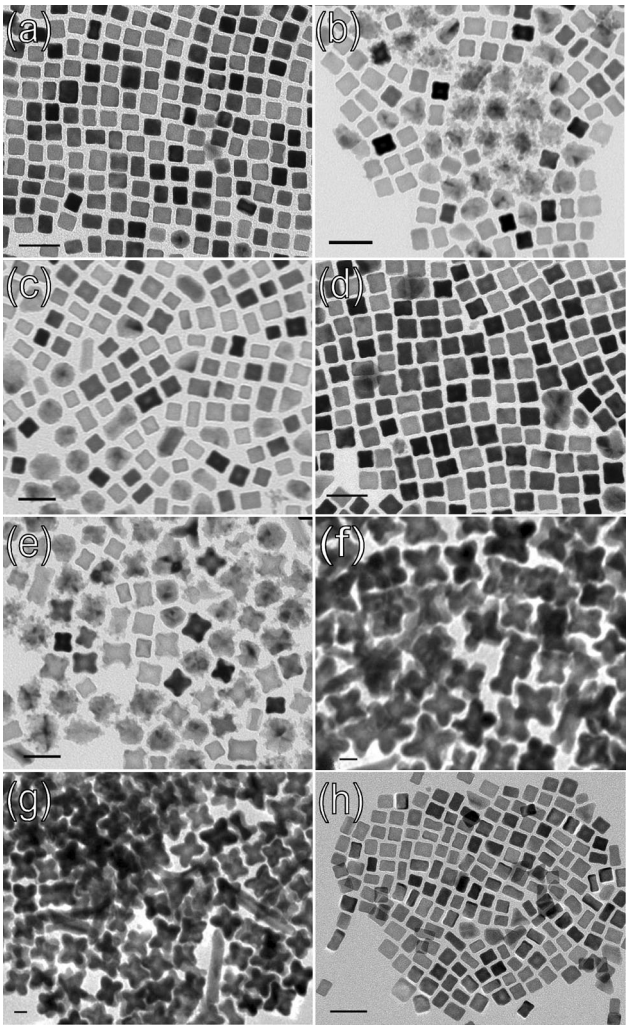

Figure 3. TEM images of Pt_3Co NCs prepared in typical experimental conditions with the following exceptions: a)–e) OAM/OA volume ratio 4:1, 6:1, 8:1, 10:1, and 12:1, respectively; f) and g) OAM/OA volume ratio 10:1 and 4:1, respectively, when $[W(CO)_6]$ was replaced with $[Cr(CO)_6]$; h) $PtCl_4$ was used as the Pt precursor. All scale bars represent 25 nm.

volume ratio, selection of reducing agent and metal precursors, respectively, whereas the other synthetic conditions were kept unchanged. First, we determined that an appropriate OAM/OA ratio is essential to ensure the formation of concave structure. In our previous report,[30] we demonstrated that perfect Pt_3Co nanocubes could be prepared when the volume ratio of OAM/OA was kept 4:1. From this point, we tuned the OAM/OA ratio by gradually increasing the relative amount of OAM to 6:1, 8:1, and 10:1, harvesting different concave nanocubes when other conditions were kept the same as stated in the typical experiment preparation. Figure 3 a–d indicates that the Pt_3Co concave nanocubes could possess both optimum concavity and uniformity when the ratio was 10:1. Although a volume ratio of OAM/OA of higher than 10:1 could further increase the concavity of the products, the shape uniformity, as well as the particle quality, was significantly degraded. Under a condition of OAM/OA 12:1, as shown in Figure 3 e, some highly branched and irregularly shaped NCs can be identified from their TEM image. Next, we have alternatively investigated the influence of metal carbonyl on the formation concave structure. As was discussed previously,[30] we believe that tungsten decomposed from tungsten hexacarbonyl $[W(CO)_6]$ may play a partial role in the formation Pt-based NCs. To verify this, we substituted $[W(CO)_6]$ with chromium carbonyl $[Cr(CO)_6]$ and re-conducted this synthesis by using the recipe stated for the typical experiment. The $[Cr(CO)_6]$-based synthesis generates larger branched NCs, as illustrated in Figure 3 f. However, it is worth pointing out that the shape of $[Cr(CO)_6]$-generated NCs is similar to that of NCs taken at the end of second minute from the $[W(CO)_6]$ system (refer to Figure S3 a in the Supporting Information), and the "concavity" of the branched NC surface is much deeper than that shown in Figure 1 a. This difference will be further discussed shortly. In addition, unlike the case with $[W(CO)_6]$, in which the particle shape varies as a function of OAM/OA ratio, the concavity of the $[Cr(CO)_6]$-generated NCs almost keeps the same when the volume ratio of OAM/OA was altered from 10:1 to 4:1 (Figure 3 f and g). Finally, we have surveyed different Pt precursors and explored their capability of resulting in desired NCs. When platinum(IV) chloride ($PtCl_4$) was chosen as a substitute for platinum(II) acetylacetonate $[Pt(acac)_2]$, the resultant cubic NCs were "elongated", because some rectangular TEM projection images could be observed without a detection of any concavity, independent of what the ratio of OAM/OA was tuned to (Figure 3 h).

It has been generally accepted that the formation of metal NCs in a solution phase consists of a nucleation process and

subsequent NC growth.[13,31] In the very initial stage, "free" atoms reduced from Pt and Co precursors at high temperature collide with each other, forming metal clusters. The ratio of released Pt and Co atoms is controlled by the difference of their reduction potentials at the reaction temperature, but could also be tuned by the "Pt^{2+}–W buffering interaction" through the introduced metal carbonyl, such as $[W(CO)_6]$.[30] When the concentration of metallic clusters rapidly approaches to supersaturation that exceeds a critical value, they further grow into tiny crystals with various crystallographic facets on the surfaces at a certain number of nucleation centres that are so-called "seeds".[32] Such a nucleation process of Pt and Co accompanies a color change from pinkish/light yellow to dark brown/black in the system. Because the environment of any seed is similar to all others that are formed due to the burst of precursor decomposition, additional metal atoms/clusters further promoted by a subsequent reaction will be "deposited" on the crystallographic facets of the existing seeds instead of creating new seeds, as long as the concentration of the feedstock does not exceed the critical value. Clearly, the surface interaction to a heteroatom in an organic molecule should be dependent on both the surface crystallographic facet on a seed and the heteroatom or the capping ligand. In the case of Pt_3Co NC synthesis, we propose that the final morphology of NCs could be developed through an "OAM/OA controlled binding" growth. As illustrated in Scheme 1, the reduced Pt under "Pt^{2+}–W buffering interaction" together with Co could directly nucleate into Pt-skeletonized alloy seeds, and the morphology of these seeds is governed preponderantly by the high rate of Pt/Co reduction in the nucleation stage.[30] With a binding of CO that is released from $[W(CO)_6]$ in the presence of OAM and OA with an appropriate composition,[33,34] it is possible to further facilitate Pt_3Co nanocubes.[30] However, the NC shape development could be altered by controlling the deposition location of Pt/Co atoms/clusters. This can be realized by a "selective binding" (or "controlled passivation") of OAM/OA on the surfaces of the seeds with a fine-tuned composition, because OAM and OA exhibit different capping abilities on diverse crystallographic facets. In other words, selective capping on different crystallographic facets by capping ligands could dominate the final shape of NCs in the NC growth stage. As indicated in this work, a relatively high ratio of OAM/OA favors the suppression of further crystallographic growth along $<100>$.[35] Such an anisotropic overgrowth could generate concavely structured nanocubes. To verify this mechanism, aliquots were taken at different reaction times to monitor the status of NC development when the typical synthesis was repeated. As was expected, the as-facilitated NCs taken from the reaction system at the end of the second minute after the nucleation show a branched morphology rather than spherical shape (Figure S3a in the Supporting Information). It was previously reported that a high rate of Pt reduction might be the predominant reason of forming dendritic Pt nanobranches observed in a Pt/Pd system.[36] In this Pt_3Co system, the driving force of generating branched seeds could also be attributed to the high concentration of metal clusters. Therefore, it is believed that the collected sample was probably from an early stage of the NC growth process. Figure S3b in the Supporting Information presents a TEM image of NCs taken after the end of the tenth minute of the reaction, showing almost perfect developed concave nanocubes. This implied that it should be energetically favorable for the spaces between the branches to be filled by the successively generated Pt and Co atoms that were promoted by the mild reducing environment during this growth process, leading to a transformation in a growth direction from branched to cubic morphology. In such a process, the unstable high-index facets could rapidly vanish. This growth phenomenon was also observed in Pt/Cu system previously.[37] However, such a growth direction could be slowed down and eventually ceased when the ratio of surface areas between the high-index planes and low-index planes reduces to certain level, due to the capping effects from the OAM/OA system. The OAM/OA selective binding could change the surface energy on each facet from their original values, making the growth tendency of "filling the branch spaces" no longer a thermodynamically favorable process. With a continuation of incubation up to the 30th minute, the TEM image of (100)-textured concave nanocubes shows an improved size-distribution (Figure S3c in the Supporting Information). However, the concave degree and particle size do not significantly change, indicating that the growth of concave nanocubes could mainly cease at the tenth minute, at which growth equilibrium between an elimination and preservation of the $\{hk0\}$ high-index planes has probably been achieved.

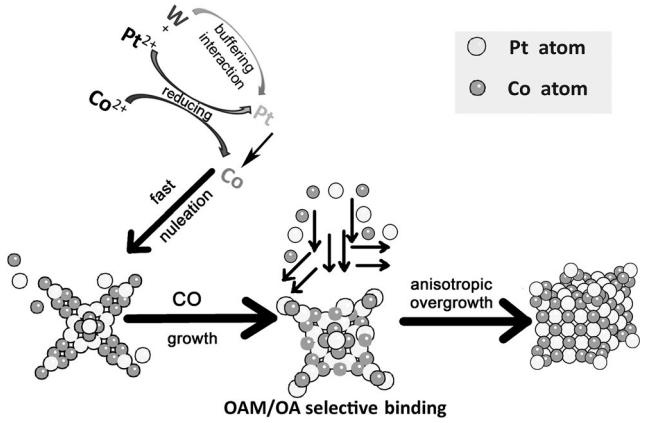

Scheme 1. Schematic illustrating a possible process of Pt_3Co concave nanocube formation.

Comprehension of the NC development process mentioned above may help us further understand why only large branched products were harvested, and no concave nanocubes could be further facilitated when $[W(CO)_6]$ was substituted with $[Cr(CO)_6]$ under the typical conditions. In comparison with W, more active metal Cr can more efficiently reduce Pt^{2+} into metallic Pt through the Pt^{2+}–Cr buffering/interaction mechanism as was discussed above, rapidly generating supersaturated Pt atoms. This will promote a more intense nucleation and therefore produce larger seeds all at once. Such a consumption of Pt atoms (synergistically with Co atoms) is expedited and completed due to the vigorous reduction of Pt^{2+},

and little Pt feedstock could be further provided to possibly alloy Co and to fill the branch space, although the coming growth process could be thermodynamically favorable. Therefore, the end of the nucleation could be the termination of the preparation with no further evolution of the NCs. The aforementioned case of $PtCl_4$ goes to another direction: tetravalent Pt precursor makes less free atoms for the nucleation. Therefore, the generated seeds should be much smaller than divalent Pt precursor does. Without sufficient exposure of various high-index planes, it will be more difficult to stop next energetically favorable growth for rapidly "filling the branch spaces" through the "selective-binding" mechanism. With sufficient feedstock in this case, eventually the high-index planes could be gone totally. Instead of generating nanocubes with concave surfaces, small NCs bounded with low-index planes, such as regular nanocubes, could be harvested. This was proved by a synthesis of $PtCl_4$-based Pt_3Co when $Pt(acac)_2$ was replaced by equal amount of $PtCl_4$ under the same experimental conditions.[38] As shown in Figure S4 in the Supporting Information, much smaller nanocubes formed as early as 30th second after the reduction of Pt^{4+} (when the solution color changes). No apparent size/shape evolution of the particles was observed.

As a typical reaction, in which unsaturated carbon–carbon bonds are broken, hydrogenation of styrene is of special importance due to its ambient conditions, high suitability to various states of catalysts, as well as many industrial demands.[39,40] As a model system under conditions of low pressure and mild coverage, this hydrogenation process has been proposed to follow a reductive-elimination step, in which addition of hydrogen that is chemisorbed on a metal surface to the olefinic substrate that is adsorbed on the same the site and subsequent generation of an ethyl intermediate are included (Scheme 2). The turnover rate is therefore believed to strongly correlate with the dissociative adsorption of H_2, activation of unsaturated bond and surface reconstruction induced by large organic adsorbates. Study on the single-crystal surfaces has suggested that stepped surface with a presence of low-coordination defect sites can readily break chemical bonds and strongly bind adsorbates.[41,42] Compared with the regular nanocubes

Scheme 2. Schematic of Pt_3Co nanocatalyst-involved styrene-hydrogenation reaction.

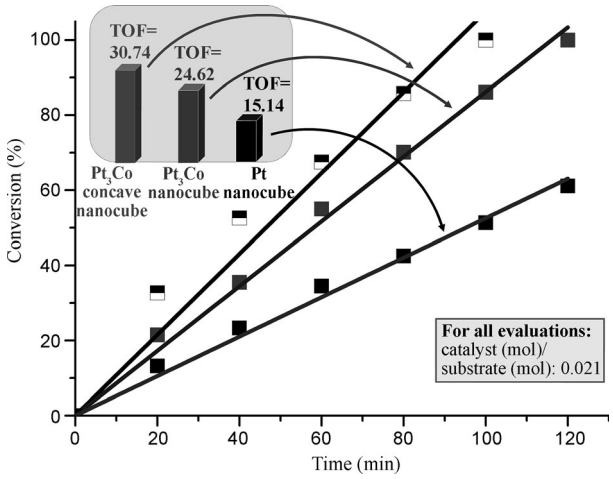

Figure 4. Conversion percentage of styrene hydrogenation as a function of reaction time by using catalysts Pt_3Co concave nanocubes and Pt_3Co nanocubes, respectively. Inset: TOFs of both catalysts in unit of [mol converted styrene]/[mol catalyst × h].

with {100}-bounded flat surface, Pt_3Co concave nanocubes with high-index planes should possess a higher catalytic activity to cleave H–H and activate C–C bonds in hydrogenation of styrene.[43] This is supported by our evaluation results of Pt_3Co concave nanocubes as shown in Figure 4. For comparison, Pt_3Co nanocubes with a similar size and composition were also prepared and studied in this investigation (Table S2 and Figure S5 a in the Supporting Information).[30,44] To monitor the reaction progress of the hydrogenation of styrene, aliquots of the reaction solution were taken in an interval of every 20 minutes and analyzed by using an NMR technique. A typical NMR spectrum showing the correlative proton information from both residue of the reactant and the converted product is presented in Figure S6 in the Supporting Information. As shown in Figure S6, feature peaks a, b, and c belong to three different olefinic hydrogen atoms in the starting material, whereas peak d is ascribed to the hydrogen atoms on the ethyl group of the product. The conversion was calculated by integrating the area of corresponding peaks. No detectable conversion of styrene was determined in the absence of Pt_3Co NCs under the experimental conditions, indicating that the Pt/Co catalysts are indispensable for facilitating this transformation. In the case of styrene, the plot of conversion versus time should be linear in most range, that is, a (pseudo-)zero-order kinetic dependence, and this was commonly observed in liquid-phase hydrogenation of olefins under a constant pressure.[3,45] The substrate (styrene) in number of moles that is converted by one mole of active catalyst within a fixed span of time can be generally described using a term of "turnover frequency (TOF)".[46,47] As a measure of catalyst activity, TOF can be derived from the conversion of starting materials as a function of time.[47] As shown in Figure 4 (inset), the TOF of the Pt_3Co concave nanocubes is 1.25 times of that for the Pt_3Co nanocubes, showing that the numbers of coordinately unsaturated atoms on their high-index surfaces of the Pt_3Co concave nanocubes could lead to an enhanced catalytic activity. Compared with Pt_3Co

nanocubes terminated with {100} planes, the concave catalysts that consist of high-index surface planes possess a lower-atom coordination numbers (see Figure 1c, e, and Figure S7 in the Supporting Information), and therefore are prone to adsorb large organic molecules with less surface reconstructions for accommodation.[15] Likewise, such kinds of surfaces with low-coordinated atoms as more catalytically active centres are also capable of binding molecular hydrogen with stronger chemical interaction to facilitate the reaction.[9] In addition, it indicates that an incorporation of Co into the nanocatalysts does enhance the catalytic performance toward hydrogenation of styrene. It is known that the introduced second transition metal could alter the *d*-band center on the Pt skin. This was observed from many electrochemical nanocatalytic studies and could be understood with a bifunctional mechanism.[48–50] In hydrogenation investigation, Nishihara et al. have also utilized rhodium/iron bimetallic NCs as enhanced catalysts for the hydrogenation of styrene.[51] In this work, a comparison between the Pt_3Co and pure Pt of conventional nanocubes (Figure S5 in the Supporting Information) in similar size shows an increment of approximately 63% TOF in terms of Pt_3Co versus the Pt counterpart (Figure 4). The acceleration of hydrogenation transformation might be attributed to the synergistic electronic effect of the Pt/Co bimetallic nanocatalysts.

The reusability test was carried out by using Pt_3Co concave nanocubes separated from a previous reaction system. After consecutively catalyzing this hydrogenation for 24 h, the Pt_3Co nanocatalysts remained active with 100% conversion of substrate. Post-analyses on the used concave catalysts did not show apparent changes on morphology (Figure S4 in the Supporting Information) and microstructure (Figure 2c), implying that the as-prepared Pt_3Co concave nanocubes can be employed as sustainable and recyclable catalysts in hydrogenation of olefins. ICP analysis on these concave nanocatalysts indicates that no element leaching was determined after a use of hydrogenation catalysis for 24 h, showing excellent composition stability that could also be part of the reason resulting in such a high catalytic performance (Table S2 in the Supporting Information).

Conclusion

For the first time, Pt_3Co concave nanocubes were prepared through a developed wet-chemical approach, in which the ratio between OAM and OA was finely tuned. Analysis suggests that the as-prepared concave nanocubes are terminated with high-index crystallographic planes containing a combination of several sub-facets with different {*hk*0} facets. A formation mechanism was subsequently proposed, and it is believed that the formation of Pt_3Co seeds is dependent on the concentration of free metallic atoms during the reaction, whereas the final morphology of NCs could be controlled by a selective binding using a combination of OAM and OA with an appropriate ratio during the stage of crystal growth. The catalytic performance of these bimetallic concave nanocubes in comparison with those of Pt_3Co and Pt nanocubes was also preliminarily tested by using a hydrogenation of styrene as a model reaction. The repeatable results indicate that the concave nanocubes possess an improved catalytic activity and stable composition/morphology, and cubic Pt_3Co bimetallic nanocatalysts are superior to pure Pt nanocubes towards the same reaction.[26] This study implies that the Pt_3Co nanocubes with a concave high-index surface structure could be potentially superior catalysts, serving in organic fine reactions.

Experimental Section

Chemicals

Cobalt(II) acetate tetrahydrate ($[Co(ac)_2{\cdot}4H_2O]$, 99.999%), $[W(CO)_6]$ (99.99%), OA (90%), $PtCl_4$ (98%), OAM (70%), and styrene (99%) were purchased from Sigma–Aldrich. $Pt(acac)_2$ (>48% Pt), $[Cr(CO)_6]$ (99%), anhydrous ethanol (200 proof), and anhydrous hexane (98.5%) were purchased from Alfa Aesar, STREM Chemicals, AAPER and BDH, respectively. Chloroform and $CDCl_3$ were obtained from J.T. Baker and Cambridge Isotope Laboratories, respectively. All chemicals were used without further purification.

Synthesis

Monodisperse Pt_3Co concave nanocubes were prepared by using a co-reduction of platinum(II) and cobalt(II) precursors in the presence of $[W(CO)_6]$, OAM, and OA. In a typical synthesis, $Co(ac)_2{\cdot}4H_2O$ (10.0 mg), $Pt(acac)_2$ (40.0 mg), OAM (10.0 mL), and OA (1.0 mL) were loaded into a three-neck flask equipped with a condenser and attached to a Schlenk line. After the mixture was heated to 140 °C with vigorous stirring under an argon stream, $[W(CO)_6]$ (50 mg) was introduced to the system, and the temperature was further raised to 240 °C and kept for 40 min with continuous agitation. The resultant Pt_3Co concave nanocubes were isolated by centrifugation and redispersed in hexane as a stock suspension after a purification by using anhydrous ethanol and hexane by using a standard method reported elsewhere.[30,44] To conduct a comparative study, Pt_3Co "regular" nanocubes were also prepared by using an established recipe.[30,44]

Characterization method

Nanocrystal characterization: XRD patterns were collected by using a PANalytical X'Pert X-ray powder diffractometer equipped with a $Cu_{K\alpha1}$ radiation source ($\lambda = 1.5406$ Å). ICP-OES analysis was carried out on an Optima 7000 DV ICP-OES spectrometer (PerkinElmer). An FEI Tecnai Spirit TEM operated at 120 kV was used for TEM imaging, JEOL2100F was used for collecting HRTEM image, and Hitachi 2700C was used for STEM EDS mapping and HAADF-STEM-EDS line scan (200 kV).

Catalytic-activity evaluation: The tests on hydrogenation of styrene were carried out under 1 atm hydrogen atmosphere at room temperature (RT) by using a setup similar to those described elsewhere.[52,53] To remove the residue of surfactant, Pt_3Co nanocatalysts were thoroughly cleaned by using the above-mentioned method and subsequently transferred into chloroform for certain period of ultrasonication before their activity evaluation. In a typical test, Pt_3Co nanocatalysts (12.0 mg) were loaded into a glass reaction vessel (10 mL) containing styrene (0.10 mL, ca. 0.87 mmol) under a hydrogen stream. The mixture was kept under 1 atm of H_2 and RT (ca. 25 °C) with a high-speed stirring for 100–120 min, and the hydrogenation mixtures were analyzed by ^1H NMR analysis (Bruker AC 300 MHz), after the Pt_3Co nanocatalysts were separated by centrifugation. When the ratio between catalysts (mol)/substra-

te (mol) was 0.021, TOF = [slope × 60 (min h^{-1})]/(0.021 × 100 %), in which the slopes were obtained from conversion/time linear relationship shown in Figure 4. After a careful cleaning by using the above-mentioned solvents two times, the recycled Pt_3Co nanocatalysts (12.0 mg) were applied to a reusability test with 1.5 mL of input styrene and continuously hydrogenation for 24 h (ca. 15 times of the duration for achieving 100 % conversion in fresh activity test).

Acknowledgements

This work was partially supported by Department of Energy and Analytical and Diagnostics Laboratory (ADL) at Binghamton University. The authors thank Dr. Jürgen Schulte for his assistance with NMR measurements. Dr. P. Stanley May and Dr. Mary T. Berry at University of South Dakota are gratefully acknowledged for their help in using the TEM facility that was obtained through an NSF grant (CHE-0840507). The HRTEM and STEM/HAADF-STEM-EDS studies were carried out at the Center for Functional Nanomaterials, Brookhaven National Laboratory, which is supported by the US Department of Energy, Office of Basic Energy Sciences, under contract no. DE-AC02-98CH10886.

Keywords: anisotropic overgrowth · catalytic activity · hydrogenation · nanostructures · platinum

[1] M. Neurock, *J. Catal.* **2003**, *216*, 73 – 88.
[2] S. Schimpf, M. Lucas, C. Mohr, U. Rodemerck, A. Brückner, J. Radnik, H. Hofmeister, P. Claus, *Catal. Today* **2002**, *72*, 63 – 78.
[3] B. Veisz, Z. Király, L. Tóth, B. Pécz, *Chem. Mater.* **2002**, *14*, 2882 – 2888.
[4] M. Jin, H. Zhang, Z. Xie, Y. Xia, *Angew. Chem.* **2011**, *123*, 7996 – 8000; *Angew. Chem. Int. Ed.* **2011**, *50*, 7850 – 7854.
[5] N. Tian, Z.-Y. Zhou, N.-F. Yu, L.-Y. Wang, S.-G. Sun, *J. Am. Chem. Soc.* **2010**, *132*, 7580 – 7581.
[6] F. Wang, C. Li, L.-D. Sun, H. Wu, T. Ming, J. Wang, J. C. Yu, C.-H. Yan, *J. Am. Chem. Soc.* **2011**, *133*, 1106 – 1111.
[7] Z.-Y. Zhou, N. Tian, J.-T. Li, I. Broadwell, S.-G. Sun, *Chem. Soc. Rev.* **2011**, *40*, 4167 – 4185.
[8] B. Lim, Y. Xia, *Angew. Chem.* **2011**, *123*, 78 – 87; *Angew. Chem. Int. Ed.* **2011**, *50*, 76 – 85.
[9] D. W. Goodman, *J. Catal.* **2003**, *216*, 213 – 222.
[10] P. Claus, *Appl. Catal. A* **2005**, *291*, 222 – 229.
[11] Z. Quan, Y. Wang, J. Fang, *Acc. Chem. Res.* **2013**, *46*, 191 – 202.
[12] Y. Yu, Q. Zhang, B. Liu, J. Y. Lee, *J. Am. Chem. Soc.* **2010**, *132*, 18258 – 18265.
[13] Y. Xia, Y. Xiong, B. Lim, S. E. Skrabalak, *Angew. Chem.* **2009**, *121*, 62 – 108; *Angew. Chem. Int. Ed.* **2009**, *48*, 60 – 103.
[14] S. C. Tsang, N. Cailuo, W. Oduro, A. T. S. Kong, L. Clifton, K. M. K. Yu, B. Thiebaut, J. Cookson, P. Bishop, *ACS Nano* **2008**, *2*, 2547 – 2553.
[15] I. Lee, F. Delbecq, R. Morales, M. A. Albiter, F. Zaera, *Nat. Mater.* **2009**, *8*, 132 – 138.
[16] N. Tian, Z.-Y. Zhou, S.-G. Sun, Y. Ding, Z. L. Wang, *Science* **2007**, *316*, 732 – 735.
[17] Z.-Y. Zhou, N. Tian, Z.-Z. Huang, D.-J. Chen, S.-G. Sun, *Faraday Discuss.* **2009**, *140*, 81 – 92.
[18] X. Huang, Z. Zhao, J. Fan, Y. Tan, N. Zheng, *J. Am. Chem. Soc.* **2011**, *133*, 4718 – 4721.
[19] T. Yu, D. Y. Kim, H. Zhang, Y. Xia, *Angew. Chem.* **2011**, *123*, 2825 – 2829; *Angew. Chem. Int. Ed.* **2011**, *50*, 2773 – 2777.
[20] J. Zhang, L. Zhang, S. Xie, Q. Kuang, X. Han, Z. Xie, L. Zheng, *Chem. Eur. J.* **2011**, *17*, 9915 – 9919.
[21] H. Zhang, W. Li, M. Jin, J. Zeng, T. Yu, D. Yang, Y. Xia, *Nano Lett.* **2011**, *11*, 898 – 903.
[22] C. J. DeSantis, A. A. Peverly, D. G. Peters, S. E. Skrabalak, *Nano Lett.* **2011**, *11*, 2164 – 2168.
[23] J. Wu, J. Zhu, M. Zhou, Y. Hou, S. Gao, *CrystEngComm* **2012**, *14*, 7572 – 7575.
[24] H. Zhang, M. Jin, J. Wang, W. Li, P. H. C. Camargo, M. J. Kim, D. Yang, Z. Xie, Y. Xia, *J. Am. Chem. Soc.* **2011**, *133*, 6078 – 6089.
[25] N. Tian, Z.-Y. Zhou, S.-G. Sun, *J. Phys. Chem. C* **2008**, *112*, 19801 – 19817.
[26] It should be mentioned that sometimes small amount of W could be determined from the ICP analysis due to an incomplete cleaning of the alloy nanocrystals. Because the content of W was varied from time to time (depending on intenseness of the particle cleaning), it is believed that the determined content of W was from adsobates, which should be avoided in a catalytic test.
[27] M. Chen, J. Kim, J. P. Liu, H. Fan, S. Sun, *J. Am. Chem. Soc.* **2006**, *128*, 7132 – 7133.
[28] C. Wang, H. Daimon, Y. Lee, J. Kim, S. Sun, *J. Am. Chem. Soc.* **2007**, *129*, 6974 – 6975.
[29] J. Zhang, H. Yang, J. Fang, S. Zou, *Nano Lett.* **2010**, *10*, 638 – 644.
[30] J. Zhang, J. Fang, *J. Am. Chem. Soc.* **2009**, *131*, 18543 – 18547.
[31] Y. Xiong, Y. Xia, *Adv. Mater.* **2007**, *19*, 3385 – 3391.
[32] C. B. Murray, C. R. Kagan, M. G. Bawendi, *Annu. Rev. Mater. Sci.* **2000**, *30*, 545 – 610.
[33] B. Wu, N. Zheng, G. Fu, *Chem. Commun.* **2011**, *47*, 1039 – 1041.
[34] Y. Kang, X. Ye, C. B. Murray, *Angew. Chem.* **2010**, *122*, 6292 – 6295; *Angew. Chem. Int. Ed.* **2010**, *49*, 6156 – 6159.
[35] S.-W. Chou, C.-L. Zhu, S. Neeleshwar, C.-L. Chen, Y.-Y. Chen, C.-C. Chen, *Chem. Mater.* **2009**, *21*, 4955 – 4961.
[36] B. Lim, M. Jiang, P. H. C. Camargo, E. C. Cho, J. Tao, X. Lu, Y. Zhu, Y. Xia, *Science* **2009**, *324*, 1302 – 1305.
[37] D. Xu, Z. Liu, H. Yang, Q. Liu, J. Zhang, J. Fang, S. Zou, K. Sun, *Angew. Chem.* **2009**, *121*, 4281 – 4285; *Angew. Chem. Int. Ed.* **2009**, *48*, 4217 – 4221.
[38] $PtCl_4$-based synthesis of Pt_3Co nanocrystals was carried out same to that for $Pt(acac)_2$-based synthesis described in the Experimental Section. The only difference is that $Pt(acac)_2$ was replaced by equal amount of $Pt^{IV}Cl_4$.
[39] N. Semagina, L. Kiwi-Minsker, *Catal. Rev. Sci. Eng.* **2009**, *51*, 147 – 217.
[40] B. Chen, U. Dingerdissen, J. G. E. Krauter, H. G. J. Lansink Rotgerink, K. Möbus, D. J. Ostgard, P. Panster, T. H. Riermeier, S. Seebald, T. Tacke, H. Trauthwein, *Appl. Catal. A* **2005**, *280*, 17 – 46.
[41] G. A. Somorjai, Y. Borodko, *Catal. Lett.* **1999**, *59*, 89 – 91.
[42] G. A. Somorjai, M. Yang, *Top. Catal.* **2003**, *24*, 61 – 72.
[43] G. A. Somorjai, K. R. McCrea, J. Zhu, *Top. Catal.* **2002**, *18*, 157 – 166.
[44] H. Yang, J. Zhang, K. Sun, S. Zou, J. Fang, *Angew. Chem.* **2010**, *122*, 7000 – 7003; *Angew. Chem. Int. Ed.* **2010**, *49*, 6848 – 6851.
[45] N. C. Gardner, R. S. Hansen, *J. Phys. Chem.* **1970**, *74*, 3298 – 3299.
[46] P. Dani, T. Karlen, R. A. Gossage, S. Gladiali, G. v. Koten, *Angew. Chem.* **2000**, *112*, 759 – 761; *Angew. Chem. Int. Ed.* **2000**, *39*, 743 – 745.
[47] K. A. Manbeck, N. E. Musselwhite, L. M. Carl, C. A. Kauffman, O. D. Lyons, J. K. Navin, A. L. Marsh, *Appl. Catal. A* **2010**, *384*, 58 – 64.
[48] G. A. Somorjai, J. Y. Park, *Chem. Soc. Rev.* **2008**, *37*, 2155 – 2162.
[49] M. Krausa, W. Vielstich, *J. Electroanal. Chem.* **1994**, *379*, 307 – 314.
[50] Y. Tong, H. S. Kim, P. K. Babu, P. Waszczuk, A. Wieckowski, E. Oldfield, *J. Am. Chem. Soc.* **2002**, *124*, 468 – 473.
[51] I. Nakamula, Y. Yamanoi, T. Imaoka, K. Yamamoto, H. Nishihara, *Angew. Chem.* **2011**, *123*, 5952 – 5955; *Angew. Chem. Int. Ed.* **2011**, *50*, 5830 – 5833.
[52] N. Weitbrecht, M. Kratzat, S. Santoso, R. Schomäcker, *Catal. Today* **2003**, *79 – 80*, 401 – 408.
[53] P. D. Vaidya, V. V. Mahajani, *Appl. Catal. B* **2004**, *51*, 21 – 31.

Received: May 3, 2013
Revised: November 26, 2013
Published online on December 30, 2013